Available online at www.sciencedirect.com
SCIENCE DIRECT®
Catalysis Today 93–95 (2004) 541–551
CATALYSIS TODAY
www.elsevier.com/locate/cattod

The influence of particle size on H_2-reduction, catalytic activity and chemisorption behavior of uranium oxide species dispersed in MCM-41: TPR, methanol-TPD and in situ FTIR studies

Dharmesh Kumar, S. Varma, N.M. Gupta*

Applied Chemistry Division, Bhabha Atomic Research Center, Trombay, Mumbai 400085, India

Available online 3 July 2004

Abstract

We report in this paper on the H_2-reduction and catalytic behavior of uranyl groups and nano-size crystallites of uranium oxide, co-encapsulated in the pore system of MCM-41 host matrix by employing the two alternative methods of incipient wet impregnation and the exchange of template cations. Based on the results of activity measurements, in situ IR spectroscopy and thermal programmed reduction/desorption studies we conclude that both the uranyl groups and the highly dispersed crystallites of uranium oxide in UO_x/MCM samples may independently contribute to the catalytic oxidation of organic molecules, such as methanol, the uranyl groups playing a more important role at lower reaction temperatures. We also observed that the lattice oxygen and the size of uranium oxide crystallites play a vital role, not only in the lowering of reaction onset temperature but also in deciding the nature and the reactivity of transient surface species formed during the decomposition/oxidation of methanol. Furthermore, whereas the larger size U_3O_8 crystallites helped in the growth of certain oxymethylene ($–OCH_2$) and polymerized oxymethylene ($(–OCH_2)_n$) species, additional formation of formate-type complexes was observed during the adsorption of methanol on smaller size particles. The formation of these distinct transient species accounted for the lowering of reaction temperature and the enhanced conversion of methanol to CO_2, CO and methane as a function of the decrease in uranium oxide crystallite size.

Keywords: Uranium oxide nanoparticles; Chemisorption behavior; Adsorption of methanol; TPR; TPD; FTIR and activity study

1. Introduction

We reported recently on the development of novel guest–host systems, comprising of uranyl groups and nano-size crystallites of uranium oxide species that were anchored/occluded in the mesopores of MCM-41 and MCM-48 materials [1–5]. The techniques of DR UV–vis and fluorescence spectroscopy were employed in these studies to demonstrate that the contacting of MCM-41 or MCM-48 with an aqueous solution of uranyl acetate followed by drying, resulted in the initial binding of uranyl ions at the ≡Si–OH sites of host matrix. A part of these uranyl ions converted to nanosize crystallites of U_3O_8 on subsequent calcination at appropriate temperature. The loading of uranium and the size and location of uranium oxide crystallites in a sample depended upon the method adopted for synthesis and the pore structure of the host material. In general, these crystallites were of smaller (<3 nm) and more uniformly distributed size when the samples were synthesized through the repeated cycles of incipient wet impregnation in a template-free MCM sample. On the other hand, comparatively larger size (3–15 nm) particles were formed when the template cations in a host matrix were exchanged directly with the uranyl ions. Further, whereas the U_3O_8 particles of less than 3 nm size were found to be generally located within the pore system of host material, the larger size crystallites were dispersed at the external surfaces. As discussed in an earlier study on this subject [5], such UO_x dispersion at external surface of exchange-prepared sample may result due to the restriction imposed by template cations to transport of uranyl ions within the pore system. On the other hand, when the sample is synthesized through an impregnation route, an easy access of uranyl ions within the pore system of template-free host matrix and their subsequent in situ conversion to U_3O_8 on calcination would result in the formation of very small particles (<3 nm). Using in situ

* Corresponding author. Tel.: +91 22 25505146; fax: +91 22 25505151/25519613.
E-mail address: nmgupta@magnum.barc.ernet.in (N.M. Gupta).

0920-5861/$ – see front matter © 2004 Elsevier B.V. All rights reserved.
doi:10.1016/j.cattod.2004.06.002

IR spectroscopy, we further demonstrated that the surface species formed during chemisorption of methanol at room temperature were different in the case of dispersed UO_x nanocrystallites, as compared to those formed over host MCM or on bulk U_3O_8 sample, under the identical reaction condition [6]. We observed that while room temperature exposure of MCM sample to methanol resulted in the formation of surface methoxy groups and dimethyl ether, the interaction over U_3O_8 gave rise to formation of certain formate-type complexes and oxymethylene species. On the other hand, the exposure of methanol over dispersed uranium oxide crystallites resulted in the development of certain polymerized oxymethylene, i.e. $(–OCH_2)_n$, type species [6].

The objective of present study was to further explore how the variation in uranium oxide crystallite size may influence their reduction behavior and also the nature of the transient species formed during adsorption of methanol at actual reaction temperatures. The experiments were performed on the above-mentioned two kinds of samples, viz. synthesized by template exchange method and alternately by wet impregnation route. The samples were characterized with the help of multiple techniques, the details of which are described earlier [1,3,5]. The method of temperature-programmed reduction (TPR) was employed for monitoring of the reduction behavior of different samples in the presence of hydrogen. The nature of surface species formed during interaction of methanol at different temperatures was monitored with the help of temperature-programmed desorption (TPD) and in situ FTIR spectroscopy. The catalytic activity was evaluated for decomposition and oxidation reactions of methanol, with an objective to establish a relationship between the nature of surface transient species formed over uranium oxide crystallites as a function of particle size and the corresponding reaction products formed at different stages. Parallel experiments were also performed on parent MCM-41 and bulk U_3O_8 samples, so as to examine the distinct role played by encapsulated uranium oxide species.

2. Experimental

2.1. Sample preparation and characterization

The method used for the preparation of nanosized uranium oxide species dispersed in mesoporous MCM-41 host has been described in our earlier publications [1,4,5]. In brief, the loading of uranium oxide species within the mesoporous MCM-41 was achieved using two different methods mentioned above. In case of impregnation method, uranyl acetate solution (0.1 M, 15 ml) was added slowly to 1 g of template-free MCM-41 sample (pretreated at 0.13 Pa for 6 h) and then stirred for 30 min. The resulting mass was washed with de-ionized water and it was then dried slowly at room temperature under vacuum. The sample was finally calcined in oxygen at 550 °C for 8 h. In the template exchange method, about 1.0 g of uncalcined MCM-41 was stirred with 15 ml of 0.1 molar aqueous uranyl acetate solution for half an hour, filtered, washed, dried in vacuum (initially at RT for 2 h and then at 60 °C) and then calcined at 550 °C for 1 h in nitrogen followed finally by 8 h heating in oxygen. The uranium content of the samples, as analyzed by spectrophotometry, was found to be 10.7 and 12.1 wt.% in the impregnated sample (referred in the text as IUM) and template exchanged (TUM) sample, respectively. The surface area of the host MCM-41, IUM and TUM samples was found to be 1000, 856 and 630 $m^2\,g^{-1}$, respectively. The surface area of a bulk U_3O_8 sample, obtained by calcination of uranyl acetate in air, was $\sim$6 $m^2\,g^{-1}$.

The procedure for characterization of samples by powder XRD, FTIR spectroscopy, DR UV–vis spectroscopy, N_2 sorption, TEM and XPS techniques has been described earlier in detail [2–5]. The XRD measurements were made on a Philips Analytical Diffractometer using Ni-filtered Cu Kα radiation in the 2θ-region of 10–70° and at a scan rate of 1°/min. The data were also collected in the selected 2–10° 2θ-region at a lower scan rate, so as to monitor the framework reflections carefully. The TEM pictures were taken on a Jeol, model 2000 FX instrument, operating at 120 kV. The samples for this analysis were prepared by ultrasonicating a sample of 300 mesh size in ethanol and then dispersing it on a carbon film supported on a copper grid.

2.2. Catalytic activity

The catalytic activity was monitored for the reaction of methanol using a fixed-bed down-flow tubular quartz reactor of 8 mm diameter, operating in a pulse mode. Experiments were carried out at isothermal temperatures in 25–500 °C region and at atmospheric pressure. A charge of 110 mg sample was placed in between two quartz wool plugs for each experiment, excepting in case of bulk U_3O_8 when a larger sample amount ($\sim$200 mg) was taken because of its high density and low surface area. The sample temperature was measured with a thermocouple fastened outside the reactor wall just above the catalyst bed. The catalyst was maintained under flow (30 ml min^{-1}) of purified He carrier gas and the successive pulses (10 numbers) composed of methanol + argon (1:16 mol ratio) or alternatively that of methanol + argon + oxygen (1:16:1.5 mol ratio) were introduced at a time interval of about 25 min. The effluents were analyzed on-line on a CHEMITO model-8510 gas chromatograph equipped with dual TCD and FID detectors, connected in tandem. Porapak QS (2 m length, 3 mm i.d.) or alternatively a Sperocarb (2 m, 3 mm i.d.) column was employed for separation of the products. Experiments were also performed using argon as a carrier gas in order to estimate the hydrogen produced during the reaction.

2.3. FTIR studies

The infrared spectra were recorded in transmission mode employing a JASCO-610 FTIR Spectrophotometer

equipped with a DTGS detector. A self-supporting sample pellet (80 mg, 25 mm diameter) was mounted for this purpose in a high-temperature, high-pressure, stainless steel cell, fitted with water-cooled CaF_2 optical windows and having a provision for in situ treatment of a sample under the desired temperature and pressure conditions. Three hundred scans were collected for recording of each spectrum at a resolution of 4 cm^{-1} in order to achieve a good signal to noise ratio. Prior to its exposure to methanol, the sample pellets were heated for 24 h in a vacuum of about 0.013 Pa at a temperature of 300 °C. The experiments were carried out by exposing a sample wafer to a mixture of methanol vapor + argon (1:16 mol ratio), while maintaining the sample at an isothermal temperature in 25–300 °C region. The final spectra were plotted after subtraction of IR bands due to un-adsorbed methanol, if any. The values given in the parentheses in some of the IR spectra represent the absorbance values that are indicative of the relative intensities of individual bands.

2.4. Temperature-programmed reduction (TPR) and temperature-programmed desorption (TPD) studies

TPR and TPD profiles were recorded on a TPDRO-1100 instrument (Thermoquest, Italy), equipped with a thermal conductivity detector and coupled on-line to a Quadrupole mass spectrometer (Omnistar 200, Pfeiffer Vacuum). For recording of a TPD profile, a 50 mg aliquot of sample was placed in a quartz microreactor, pretreated at 550 °C under He flow (30 ml min^{-1}) for 24 h and then cooled to room temperature. Around forty number pulses (10 ml each) of 5% methanol in argon were then dosed over the sample, while maintaining it under He flow (10 ml min^{-1}). The catalyst was then purged with He (20 ml min^{-1}) for one hour in order to remove the physisorbed methanol. A TPD run was recorded in 25–550 °C temperature region at a ramping rate of 10 °C min^{-1}. The effluents from the reactor were continuously monitored by TCD and QMS as a function of temperature.

TPR profiles were similarly recorded in the flow of H_2 (5%) + Ar (20 ml min^{-1}) and at a heating rate of 6 °C/min. The effluent was passed through a soda lime trap to remove the water formed during the reaction. Prior to recording of a profile, the sample was calcined in air at 600 °C and then subjected to in situ pretreatment, first in oxygen flow (550 °C, 1.5 h) and then in helium (550 °C, 1.5 h).

3. Results and discussion

3.1. Sample characteristics

The method of preparation had profound influence on the physico-chemical characteristics of the samples, as monitored by XRD, N_2 sorption, DR UV–vis, FTIR and XPS techniques. As mentioned above, the sorption of uranyl acetate followed by drying in air resulted in the anchoring of uranyl ions within the pores of MCM-41 host matrix, both in case of IUM and TUM samples. A part of these uranyl groups converted to U_3O_8 crystallites on subsequent calcination in air (at 550 °C), as revealed by DR UV–vis results [5]. Even though both the uranyl groups and U_3O_8 crystallites existed together in both kinds of samples, the size of U_3O_8 particles was found to be quite different. For instance, curves a and b in Fig. 1 show typical XRD patterns of samples TUM and IUM, respectively, recorded in 10–70° 2θ-region. Curves d and e in the inset of this figure show the comparative patterns of TUM and IUM samples in 2–10° 2θ-region and these XRD patterns reveal that the long range ordering of the host matrix is preserved to a good extent in the case of both the samples. The XRD reflections appearing at *d*-values of 4.15, 3.40, 2.62, 2.07, 1.96, 1.75 and 1.59 Å in curve a in Fig. 1 correspond closely to {0 0 1}, {0 3 1}, {1 3 1}, {2 0 0}, {0 3 3}, {1 3 3} and {1 6 2} reflections of α-U_3O_8 [JCPDS card no. 24-1172]. The average particle size of these uranium oxide crystallites in TUM sample was found to be ~10 nm, as calculated using Scherrer equation. On the contrary, we see only a broad XRD profile in this 2θ-region in the case of sample prepared through impregnation route (curve b in Fig. 1). This is ascribed to high dispersion of uranium oxide species in this case, mostly within the pores of host material. Such a phenomenon has been reported by other researchers for metal oxides dispersed in mesoporous materials [7,8]. In support of these XRD data, typical TEM pictures of TUM and IUM samples taken along the pore axis are presented in Fig. 2a and b, respectively. These pictures exhibit the hexagonal pore structure of host MCM-41 [9] and at the same time reveal some disordering

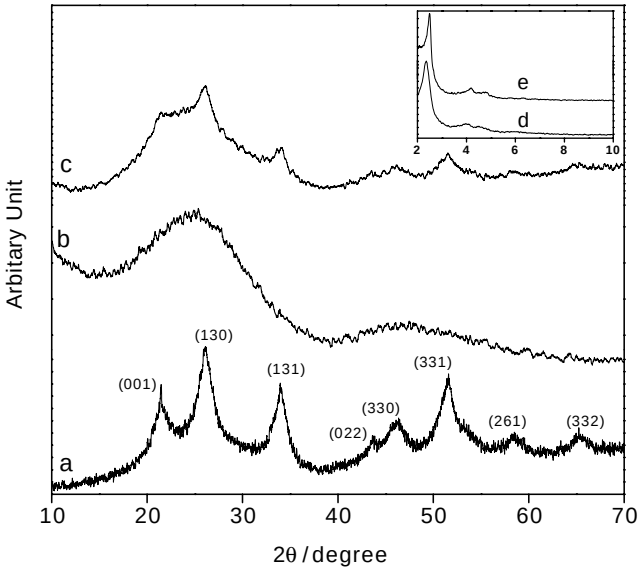

Fig. 1. Effect of calcination on XRD pattern of TUM (a) and IUM (b, c) samples. Calcination temperature: curves (a, b) 550 °C, curve (c) 800 °C. Inset figure shows XRD patterns of (d) TUM and (e) IUM samples in 2–10° 2θ-region.

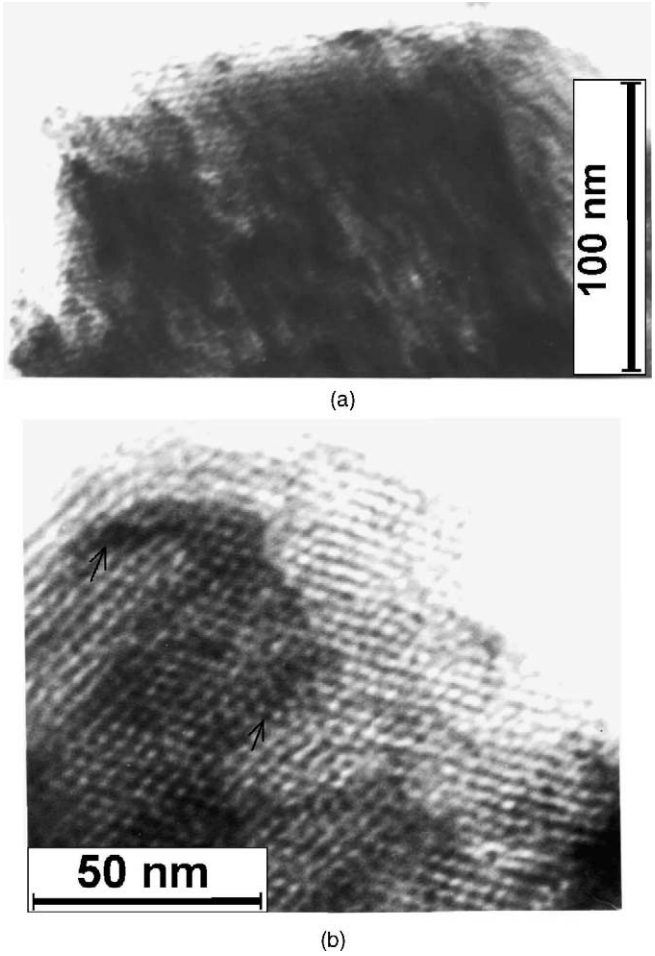

Fig. 2. TEM monograph of (a) TUM and (b) IUM sample, along pore axis.

in the pore structure. It is of further interest to notice that the uranium crystallites are more uniformly distributed in the case of IUM samples, as is evident from the difference in the contrast of some of the pores (marked with the arrows). We also observe in Fig. 2b that the particles of size $\leq$3 nm are located mostly within the mesopores of host matrix. On the other hand, a wider range of particle size distribution (2–15 nm) is noticeable in the case of TUM where large size particles are dispersed at the external surface of the host material (Fig. 2a). This is in accordance with the XRD results of curve a in Fig. 1. The bar graphs in Fig. 3a and b give the size distribution of uranium oxide crystallites in TUM and IUM samples, respectively.

The above inference regarding the comparatively higher dispersion of UO_x species at the external surface of TUM sample gets validated when we compare the U/Si ratio at the surface of two samples, as determined by XPS measurement. These results are presented in Table 1. TUM sample shows a very high U/Si ratio of about 7.3 compared to a corresponding value of 0.7 in case of IUM sample. The detailed results on XPS studies are given elsewhere [5]. The temperature at which a sample was calcined subsequent to soaking in uranyl solution followed by drying also had a

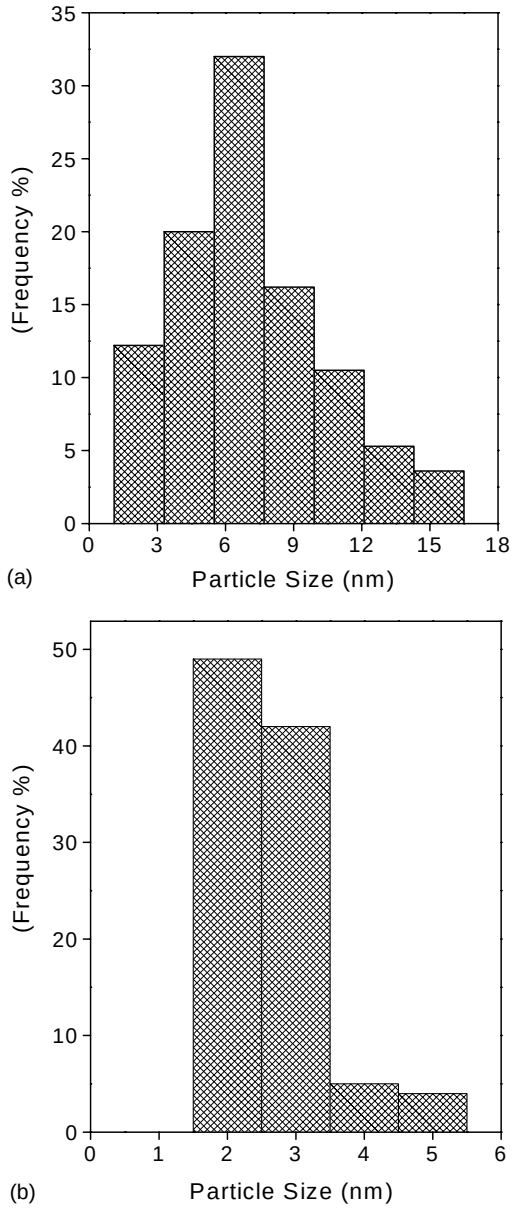

Fig. 3. Plots (histograms) showing particle size distribution in (a) TUM and (b) IUM sample, as arrived from TEM results.

strong influence, the extent of $UO_2^{2+} \rightarrow U_3O_8$ conversion and the size of U_3O_8 particles increasing considerably at high calcinations temperatures. In order to show this trend, curve c in Fig. 1 presents the XRD pattern of an IUM sample, recorded on calcination at 800 °C instead of 550 °C (cf.

Table 1
XPS data for bulk U_3O_8, IUM and TUM samples

Sample	BE (eV)		FWHM for $4f^{7/2}$ signal	U/Si
	$4f^{7/2}$	$4f^{5/2}$		
IUM	381.6	392.2	3.7	0.73
TUM	381.7	392.2	2.8	7.2
U_3O_8	381.5	392.1	2.7	–

curve a in Fig. 1), indicating the prevalence of α-U_3O_8 crystallites (average particle size ∼7 nm).

3.2. Catalytic activity

The methanol was found to adsorb strongly in host MCM-41 material but its conversion to reaction products was rather small. Thus, at a typical temperature of 500 °C, a conversion of only ∼11 mol% of dosed methanol was observed, and CO, CO_2 and dimethyl ether were the main reaction products. The bulk U_3O_8 on the other hand exhibited poor adsorption of methanol due to small surface area and again only a small fraction of adsorbed methanol was found to react at temperatures below 500 °C. In this case, while CO and CO_2 were the main reaction products at higher temperatures, the formation of ∼2–5 mol% of organics (formaldehyde, dimethoxy methane and methyl formate) was observed at temperatures in region 25–200 °C. The typical temperature dependent catalytic activity data for MCM-41 and bulk U_3O_8 samples are given in Fig. 4A and B, respectively. The corresponding results on the samples IUM and TUM are presented in Fig. 5A and B, respectively. As observed in these figures, CO and CO_2 were the main reaction products with the yield of CO being greater than that of CO_2, and no measurable quantities of organic products were formed on both these samples. In addition, the formation of small amounts of CH_4 and H_2 was also observed at temperatures above 300 °C. Further, as compared to TUM, the percentage conversion of methanol was always higher in the case of sample IUM. Thus, a maximum conversion

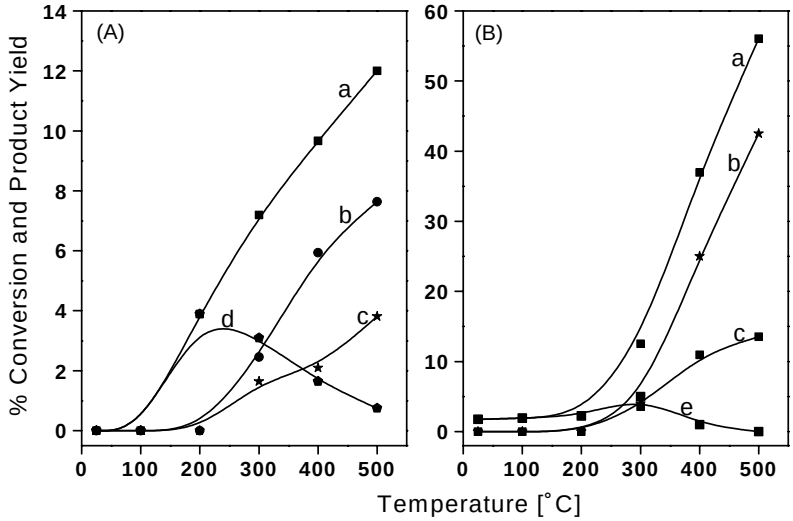

Fig. 4. Temperature-dependent yield of different reaction products formed during exposure of CH_3OH over (A) MCM-41 and (B) bulk U_3O_8 catalyst samples. (b) CO, (c) CO_2, (d) dimethyl ether, and (e) organics. Curve (a) represents the % conversion of methanol.

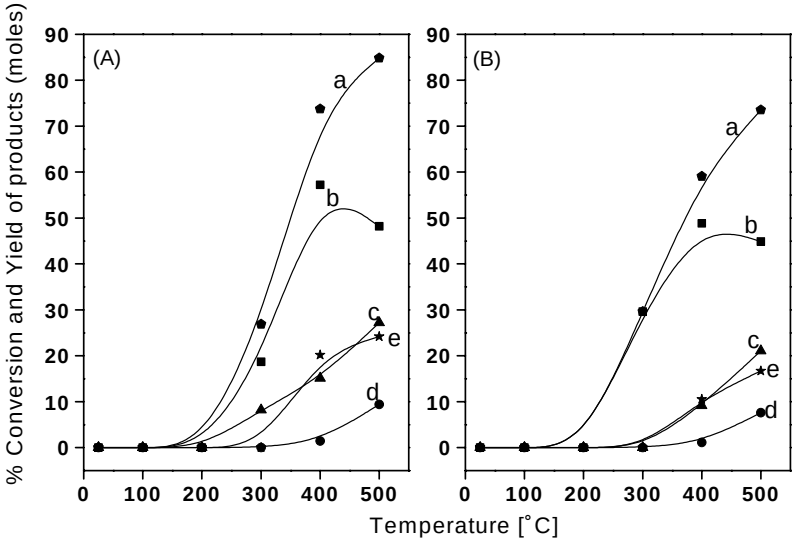

Fig. 5. Temperature-dependent yield of different reaction products formed during exposure of CH_3OH over (A) IUM and (B) TUM catalyst samples. (b) CO, (c) CO_2, (d) CH_4 and (e) H_2. Curve (a) represents the % conversion of methanol.

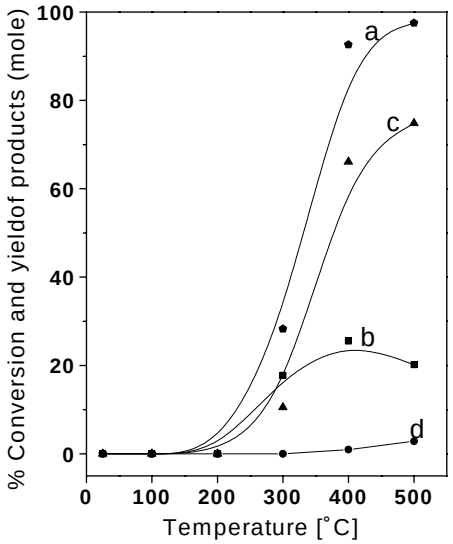

Fig. 6. Temperature-dependent yields of reaction products formed during exposure of $CH_3OH + O_2$ over IUM catalyst sample (b) CO, (c) CO_2 and (d) CH_4. Curve (a) represents the % conversion of methanol.

to the extent of about 86% and 74% was observed in the case of samples IUM and TUM, respectively, at a typical reaction temperature of 500 °C (curve a). Also, the onset temperature for the formation of CO_2 was comparatively lower in case of sample IUM, and at the same time the ratio CO_2/CO was always higher (Fig. 5, curves b and c). The conversion of methanol increased significantly when methanol + oxygen were reacted on both the samples, the yield of CO_2 increasing at the expense of CO and CH_4. Typical activity data for the reaction of $CH_3OH + O_2$ over IUM sample are presented in Fig. 6. The difference in the activity behavior in case of IUM and TUM samples in spite of their similar uranium content and also the different reaction products formed on bulk U_3O_8 and UO_x/MCM samples may thus be related to the effect of particle size.

3.3. In situ FTIR studies on adsorption/reaction of methanol

In order to identify the individual reaction steps responsible to different catalytic properties of TUM, IUM, U_3O_8 and MCM-41 samples as described above, and to discriminate between the transient species formed during the interaction of methanol on theses sample, in situ FTIR studies were performed at various reaction temperatures. The parallel studies carried out under room temperature conditions have been described in our earlier work [6].

3.3.1. Adsorption of methanol over MCM-41 and bulk U_3O_8

Curves a and b in Fig. 7 present the IR bands of MCM-41 in two different regions after exposure to 54 μmol of methanol at 25 and 200 °C, respectively. As seen in curve a in Fig. 7, the adsorption of methanol over MCM-41 gave rise to prominent bands at 2956 and 2846 cm^{-1}, related to asymmetric and symmetric stretching vibrations of widely reported methoxy (–OCH_3) groups [10,11]. The 1465 cm^{-1} band in this figure may be identified with the corresponding C–H bending vibration. The bands at 2994 and 1444 cm^{-1} along with the overlapping bands in 1360–1330 cm^{-1} region in this figure may be attributed to the presence of condensed and adsorbed methanol [10,11]. Another band at

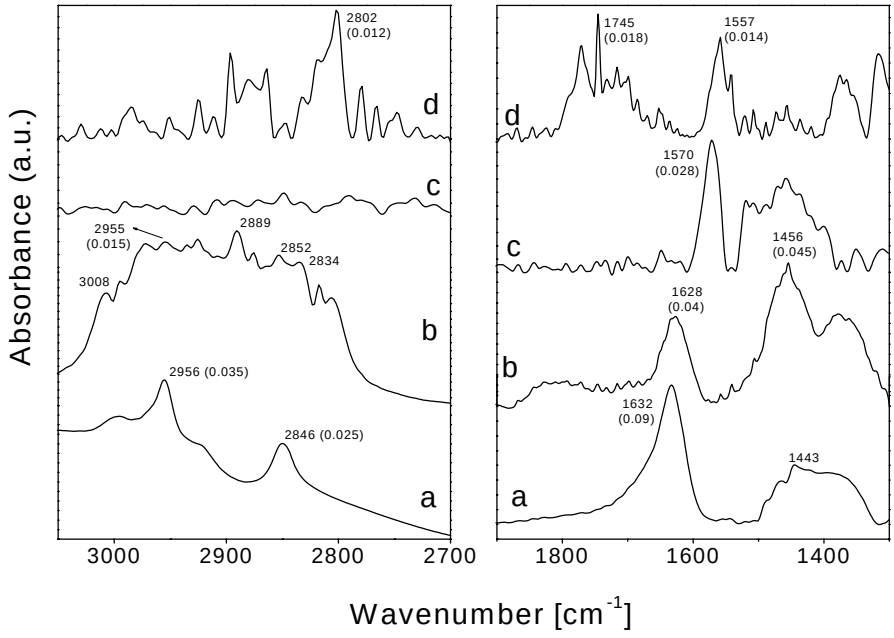

Fig. 7. IR spectra of sample MCM-41 (curves a, b) and U_3O_8 (curves c, d), after contact with 54 μmol of methanol at two different temperatures, curves (a, c) 25 °C and curves (b, d) 200 °C. The values in parentheses represent the relative absorbance values.

1632 cm^{-1} is typical deformation mode vibration of water molecules that are formed during the reaction. Because of the absence of associated rotational bands, it is surmised that the water molecules are in an adsorbed state.

The IR bands due to methoxy species were found to decrease in intensity (as seen from absorbance values given in parentheses) with the progressive increase in reaction temperature (curve b in Fig. 7). At the same time, ν(C–H) bands due to dimethyl ether at around 3008, 2996, 2985, 2932, 2914, 2903, 2889, 2879, 2834, 2817 and 2805 cm^{-1} and corresponding δ(C–H) bands at about 1454 and 1473 cm^{-1} are observed, the intensity of which increased on further rise in temperature. It is envisaged that the formation of dimethyl ether occurs during interaction of methoxy groups with free CH_3OH molecules at higher temperatures [12]. Also observed in curve b in Fig. 7 are a number of rotational bands in 1900–1500 cm^{-1} region associated with 1634 cm^{-1} band, indicating the release of water vapor.

Curves c and d in Fig. 7 show the surface species formed over bulk U_3O_8 on methanol adsorption. The major species formed in this case during room temperature adsorption are represented by 1570 cm^{-1} band, which is a characteristic stretching vibration of unidentate formate ($–COO^-$) species bonded to metal sites. The formation of such species has been reported earlier for the adsorption of methanol on other metal oxides also [13–15]. The overlapping bands observed in frequency region of 1550–1370 cm^{-1} in curve c in Fig. 7 may be identified with oxymethylene ($–OCH_2$) groups, as discussed in our earlier publication [6]. We thus infer that the interaction of methanol with uranium oxide results in its dehydrogenation to give formaldehyde in adsorbed state, which in turn on oxidation yields the formate-type species.

Curve d in Fig. 7 shows the corresponding spectrum recorded after exposure of methanol over U_3O_8 at 200 °C. The prominent ν(C–H) stretching region bands in 2950–2730 cm^{-1} in curve d in Fig. 7 match well with the C–H stretching bands of formaldehyde. Similarly, the prominent bands at 1771, 1745 and 1716 cm^{-1} correspond to the PQR branching of the formaldehyde carbonyl groups [16]. In addition to the above-mentioned species, also observed were the bands due to CO and CO_2 in 2400–2000 cm^{-1} region (not shown in this figure). These results thus reveal that the formate and oxymethylene species (curve c in Fig. 7) transform at elevated reaction temperatures to produce formaldehyde and the oxides of carbon as main products [16].

3.3.2. Adsorption of methanol over IUM and TUM samples

As compared to above-mentioned results on bulk U_3O_8 sample (curves c and d in Fig. 7), a significant difference was noticed in the nature of the transient species formed and also in the reaction onset temperature when CH_3OH was dosed on UO_x/MCM samples. Figs. 8 and 9 depict the transmission IR spectra in the C–H stretching and bending modes of methanol, when samples TUM and IUM were exposed to 54 μmol of methanol at different temperatures in 25–300 °C region. Following picture emerges from the results exhibited in these figures. We observe in curve a in Figs. 8 and 9 the C–H stretching (∼2956, 2848 cm^{-1}) and C–H bending (1465 cm^{-1}) region vibrational bands arising due to methoxy groups, formed on interaction of CH_3OH with silicate host at room temperature (cf. curve a in Fig. 7). The band at 1444 cm^{-1} along with the overlapping bands in 1400–1330 cm^{-1} region are typical of adsorbed methanol. The corresponding stretching region IR bands of adsorbed methanol overlap with those due to methoxy groups [10,11].

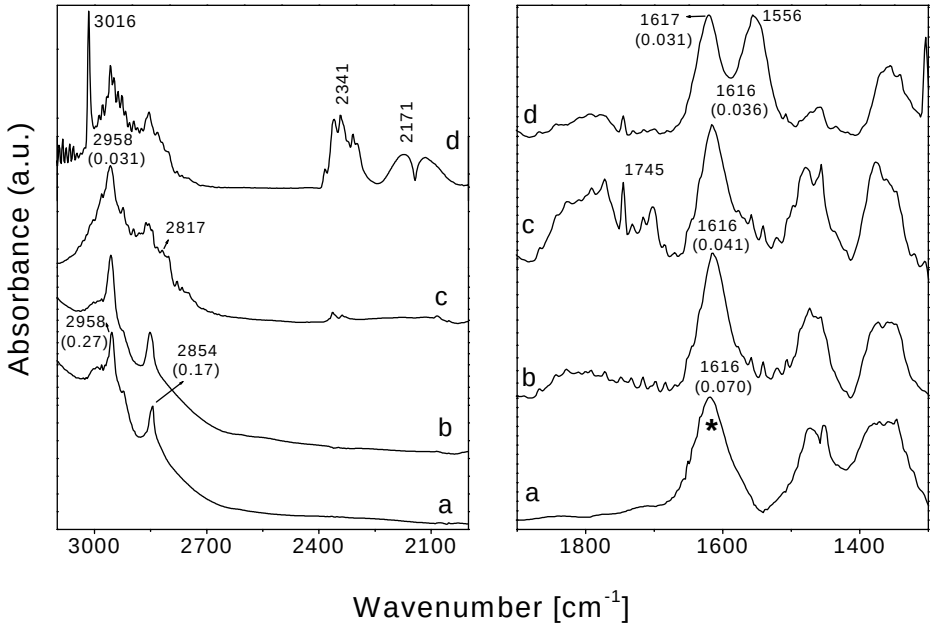

Fig. 8. IR spectra of sample TUM, after contact with 54 μmol of methanol at different temperatures: (a) 25 °C, (b) 100 °C, (c) 200 °C and (d) 300 °C.

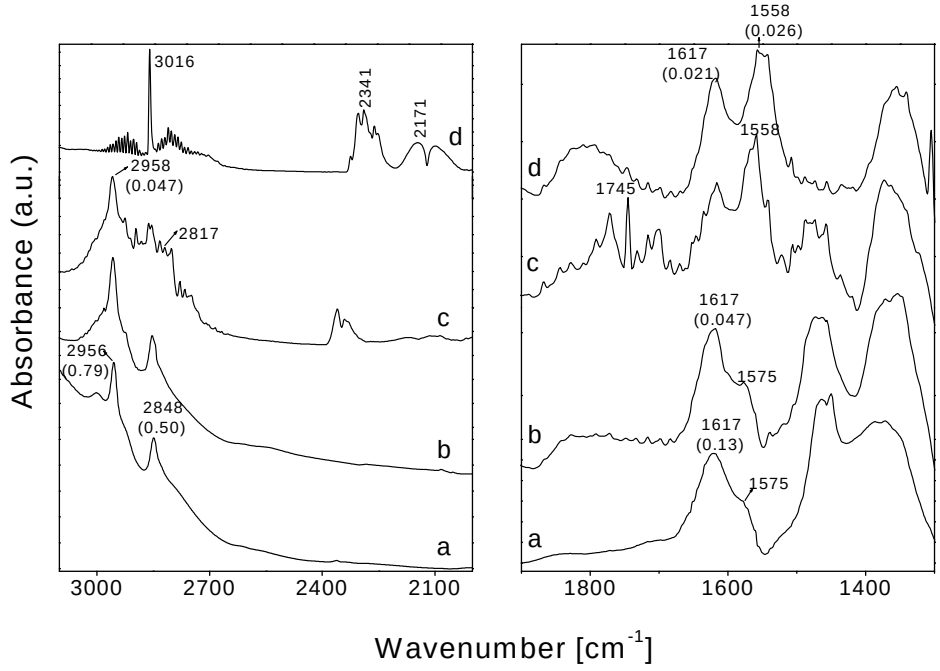

Fig. 9. IR spectra of sample IUM, after contact with 54 μmol of methanol at different temperatures: (a) 25 °C, (b) 100 °C, (c) 200 °C and (d) 300 °C.

In addition, a strong band observed at 1616 cm^{-1} along with shoulders at 1644 and 1652 cm^{-1} in the C–H bending region in and a group of weak bands in the 3050–2950 cm^{-1} region in Figs. 8 and 9 are those corresponding to the bending and stretching region vibrations of polymerized oxymethylene species $(–OCH_2)_n$, formed due to interaction and dehydrogenation of methanol over dispersed uranium oxide crystallites.

The assignment of above-mentioned vibrational bands in 1650–1610 cm^{-1} region to polymerized oxymethylene $(–OCH_2)_n$ species was based on our experiments on adsorption of formaldehyde on UO_x/MCM samples, as is discussed in detail in Ref. [6]. In brief, the identical bands in the region 3050–2900 and 1650–1600 cm^{-1} were also observed when formaldehyde vapor were dosed over UO_x/MCM samples at room temperature. These $(–OCH_2)_n$ species were found to be stable on pumping of the sample at ambient temperature, and gave rise to release of free formaldehyde along with the reaction products such as CO and CO_2 on subsequent raising of sample temperature. It is of interest to notice that the intensity of these bands (marked with ∗) is almost two times greater in case of IUM sample (curve a in Fig. 9) as compared to that on TUM (curve a in Fig. 8), as is revealed by the absorbance values given in parentheses. Further, in case of curve a in Fig. 9, we also observe an additional IR band at about 1575 cm^{-1}, not seen in curve a in Fig. 8, and this is typical of the unidentate formate complex species [14–16]. These formate species may form as a result of further oxidation of above-mentioned oxymethylene and poly-oxymethylene species at uranium sites.

At elevated reaction temperatures of 100 and 200 °C, we observe the presence of new bands in both the stretching and the bending regions of C–H vibration in curves b and c in Fig. 8 and also in curves b and c in Fig. 9. As in curve d in Fig. 7, we observe a number of overlapping vibrational bands in 2925–2748 cm^{-1} region corresponding to C–H stretching bands of formaldehyde and also the bands at 1772, 1745 and 1716 cm^{-1} along with the shoulders at 1791, 1731 cm^{-1} that are typical PQR vibrations of carbonyl group in formaldehyde [6,16]. A simultaneous decrease in the intensity of IR bands due to above-mentioned polymerized oxymethylene species is observed in case of both the samples, indicating that a part of these species convert to form of formaldehyde. In addition, we observe in curve c in Figs. 8 and 9 a prominent IR band at 1575 cm^{-1} due to unidentate formate species (–OOCH), and also a vibrational band at 1558 cm^{-1} attributed normally to bidentate formate species (=OOCH) [16]. Comparing the data in these two figures, the intensity of these formate bands is found to be very weak in case of TUM sample (curve c in Fig. 8). The bands due to these formate complex species are found to grow with the rise in sample temperature and in case of IUM sample their concentration at sample temperature of 200 °C is even greater than that of the polymerized oxymethylene species indicating thereby a partial conversion of polymerized species to formate complex species. Further, the bands are also noticed in the 2400–2100 cm^{-1} region, which are attributed to the formation of CO and CO_2 and again the intensity of these bands was found to be considerably higher in case of the sample IUM as compared to TUM.

With further rise in temperature to 300 °C, we observe the formation of methane (3016 cm^{-1} and a number of rotational bands) along with the increase in the intensity of bands due to CO and CO_2. We also notice a simultaneous

decrease in the intensity of bands arising due to polymerized oxymethylene species and formate complex species. A complete decomposition of formaldehyde is thus seen clearly in case of sample IUM (curve d in Fig. 9) in contrast to corresponding data in curve d in Fig. 8.

Thus, based on the above results it is quite evident that the chemisorption behavior of bulk U_3O_8 and dispersed UO_x species is quite different. Thus, while room temperature adsorption over bulk U_3O_8 resulted in the formation of formate complex and oxymethylene species, the exposure of methanol over UO_x/MCM gave rise to surface-adsorbed $(–OCH_2)_n$ type polymerized species. These surface transients undergo further oxidation/decomposition reactions to give rise to CO, CO_2 and CH_4 as final products; the size of UO_x crystallites having a strong influence on these transformations. The results of Figs. 8 and 9 clearly reveal that the smaller size crystallites of uranium oxide (∼3 nm) in sample IUM exhibited better oxidizing activity compared to those of larger size (2–15 nm) on sample TUM. Overall, the IR studies thus demonstrate that various intermediates, such as oxymethylene, poly-oxymethylene and the formate-type complex species, play a vital role in the overall processes of decomposition and oxidation of methanol and the surface transformations that they undergo under particular reaction conditions are governed by the morphology of the dispersed UO_x species.

3.4. Temperature-programmed reduction

Fig. 10 presents the TPR profiles of bulk U_3O_8, uranium-free MCM-41, IUM and TUM samples. As expected, no hydrogen consumption is observed during the TPR cycle of host MCM-41 material (curve a in Fig. 10). U_3O_8, on the other hand, undergoes a single step reduction as shown in curve b in Fig. 10, the temperature of peak maximum being at ∼640 °C. A weak shoulder band at ∼510 °C is also noticeable in this figure. XRD pattern of spent sample, recovered after a TPR cycle, indicated the transformation of U_3O_8 to UO_2 species. TPR profile of samples IUM and TUM are given in curves c and d of this figure. In case of both the samples we observe two reduction stages. For IUM sample these reduction stages are observed at temperatures of 510 and 575 °C, whereas for TUM samples we observe TPR peaks at 520 and 600 °C. The peaks observed at 510 and 520 °C in case of IUM and TUM samples are attributed to reduction of uranyl groups whereas the peaks observed at 575 and 600 °C are ascribed to reduction of U_3O_8. It is of interest to observe in these data that the intensity of TPR band corresponding to uranyl groups is much higher in case of IUM (curve c in Fig. 10), as compared to TUM sample (curve d in Fig. 10). These observations are in line with our finding that the content of uranyl group is higher in case of IUM sample compared to TUM, even though samples were prepared under the same condition of calcination. Our assignment of 510 and 575 °C TPR bands to reduction of uranyl groups and U_3O_8 species, respectively, finds support when we compare the TPR plots of an IUM sample calcined at two different temperatures, i.e. 550 °C (curve c in Fig. 10) and 800 °C (curve e in Fig. 10), respectively, since the high temperature calcination resulted in larger size crystallites of U_3O_8 (see curve c in Fig. 1). The change in the relative intensity of above-mentioned TPR bands in curves c and e of Fig. 10 is thus in agreement with our inferences.

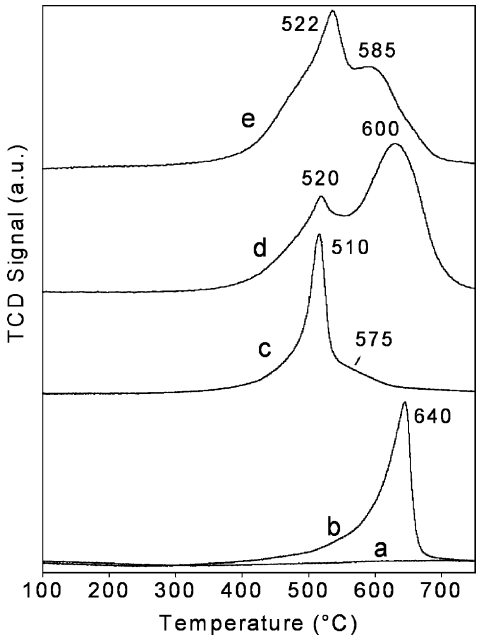

Fig. 10. TPR profiles of (a) MCM-41, (b) U_3O_8, (c) IUM, (d) TUM samples calcined at 550 °C. Curve (e) represent the TPR profile of IUM sample calcined at 800 °C.

3.5. Temperature-programmed desorption

Fig. 11 shows typical temperature-programmed desorption (TPD) profiles, obtained after room temperature adsorption of methanol on host MCM-41 and IUM samples. A parallel experiment on bulk oxide sample gave no desorption signal, indicating only negligible adsorption of methanol over low surface area U_3O_8. TPD spectrum in Fig. 11A for adsorption of methanol over siliceous MCM-41 shows a single broad desorption profile with a maximum temperature (T_{max}) of about 150 °C. On the other hand, we observe two well defined TPD peaks at 140 and 375 °C for adsorption of methanol over IUM sample (Fig. 11B). The QMS analysis of the desorbed species from MCM-41 and IUM samples are also presented in the respective figures. As seen in these data, the desorbed species in case of MCM-41 in the lower temperature range correspond to methanol, water, dimethylether, carbon dioxide and hydrogen. The study thus indicates that a part of methanol is weakly bound to the host sample and gets released on thermal activation. The rest interacts to form the products mentioned above. Mass spectral analysis in Fig. 11B reveals the formation of formic

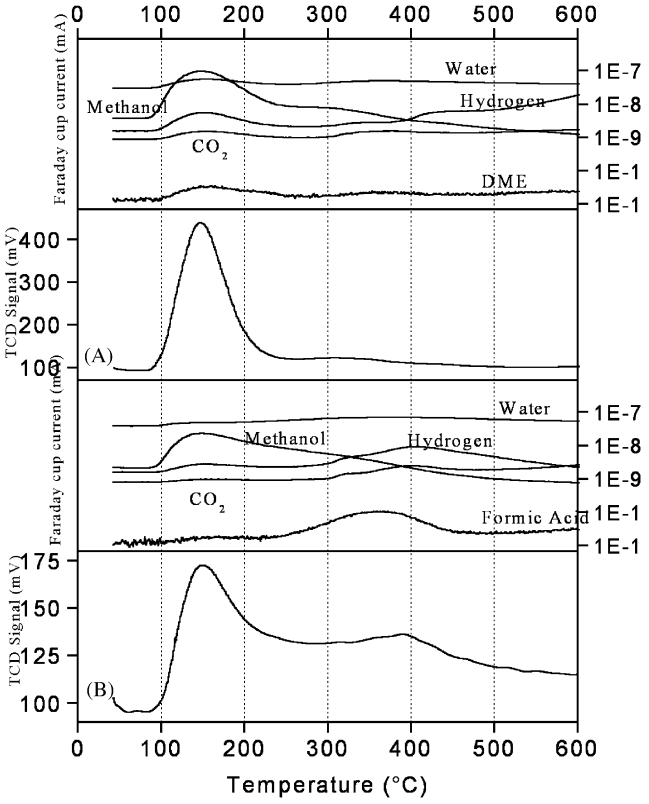

Fig. 11. TPD profiles obtained on (A) MCM-41 and (B) IUM samples after saturation coverage of methanol followed by flushing in helium. The corresponding reaction products evolved are also shown.

acid ($m/e = 45, 46$) in temperature region 300–400 °C, and simultaneously that of CO_2, H_2O and H_2. It may thus be inferred that whereas binding at framework sites of MCM is a major process at the low temperatures, a part of adsorbed methanol interacts with the dispersed uranium oxides at higher temperatures to result in the formation of different transient species, which in turn oxidize to yield the reaction products mentioned above. These TPD results are thus in perfect harmony with our IR data presented in Figs. 8 and 9. These results also help us to conclude that the UO_x species serve as a reversible source of oxygen that promotes these oxidation steps.

4. Summary

Based on the results of activity measurements, IR and thermal programmed reduction studies we can conclude that both the uranyl groups and the highly dispersed crystallites of uranium oxide in U/MCM samples may independently contribute to the catalytic oxidation of organic molecules, such as methanol. Further, the uranium oxide crystallites not only serve as independent reaction sites but the bulk oxygen and the size of the particles also plays an important role in deciding the nature and reactivity of the transient surface species formed during decomposition/oxidation of methanol. The picture that emerges from the results of present study on the reaction of methanol over UO_x/MCM (Figs. 7–9) is presented in Scheme 1. Thus, the interaction

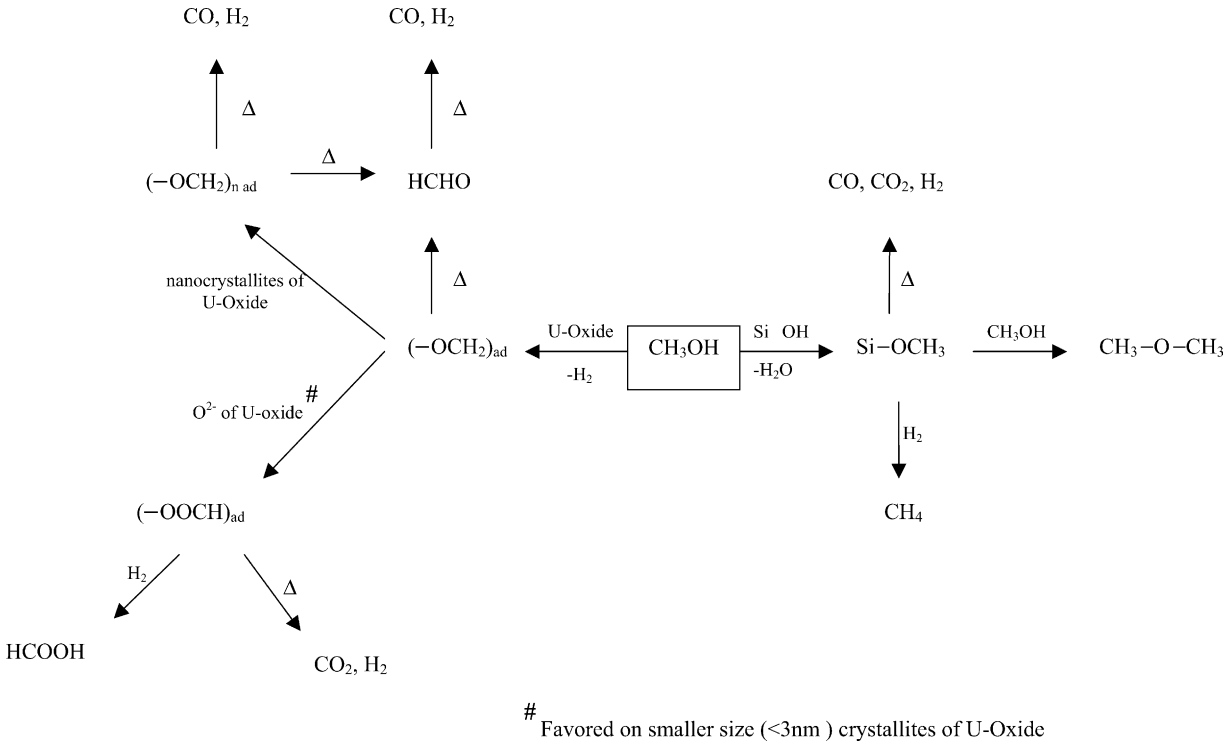

Scheme 1. Steps involved in reaction of CH_3OH over UO_x/MCM catalyst.

of methanol with silanol groups results in the formation of methoxide species which may transform to give dimethyl ether or methane or alternatively may decompose at elevated temperatures to produce the oxides of carbon (Figs. 8, 9 and 11), as shown in Scheme 1. On the other hand, the interaction with uranium oxide species results in dehydrogenation of methanol molecules, so as to give rise to formation of oxymethylene groups, which polymerize further to produce poly-oxymethylene species. We observe in Figs. 8 and 9 that the polymerization process occurs to a relatively greater extent on the IUM sample consisting of highly dispersed UO_x crystallites, as compared to sample TUM. Further, the high temperature IR results demonstrate that the oxymethylene and poly-oxymethylene species further undergo partial oxidation to give rise to formate complex species; the smaller size oxide crystallites (3 nm and less) favoring such a process as compared to somewhat larger size particles (2–15 nm). These results are in agreement with the TPD results of Fig. 11, showing clearly the involvement of UO_x moieties in formation of various surface species giving rise eventually to formic acid and other products on oxidation, where the lattice oxygen may play an important role.

The TPR results of Fig. 10 provide an important clue as regards to the role played by bulk oxygen in the oxidizing characteristics of UO_x moieties. It is observed that the uranyl groups anchored on to the walls of MCM-41 are amenable to reduction in temperatures region of 350–550 °C, as compared to U_3O_8 that reduces at higher temperatures (curve b in Fig. 10). In addition, the temperature at which U_3O_8 crystallites undergo H_2 reduction depends upon the particle size also, the smaller the size the lower is the reduction temperature (Fig. 10). It is thus evident that the relative contribution of uranyl groups and U_3O_8 sites in the overall catalytic oxidation reaction may depend upon the reaction temperature; the uranyl groups playing more important role initially and the contribution of U_3O_8 particles increasing with rising temperature.

Over all, we may thus conclude that the presence of uranyl groups, the lattice oxygen and the size of U_3O_8 crystallites together play a vital role, not only in lowering of the reaction onset temperature but also in deciding the nature and reactivity of the transient surface species formed during adsorption/oxidation of methanol, thus influencing the kinetics and the selectivity of the reaction.

References

[1] K. Vidya, S.E. Dapurkar, P. Selvam, S.K. Badamali, N.M. Gupta, Micropor. Mesopor. Mater. 50 (2001) 173.
[2] K. Vidya, S.E. Dapurkar, P. Selvam, S.K. Badamali, D. Kumar, N.M. Gupta, J. Mol. Catal.: Chem. 181 (2002) 91.
[3] D. Kumar, K.T. Pillai, V. Sudersanan, G.K. Dey, N.M. Gupta, Chem. Mater. 15 (2003) 3859.
[4] D. Kumar, S. Bera, A.K. Tripathi, G.K. Dey, N.M. Gupta, Micropor. Mesopor. Mater. 66 (2003) 157.
[5] D. Kumar, G.K. Dey, N.M. Gupta, Phys. Chem. Chem. Phys. 5 (2003) 5477.
[6] D. Kumar, V.S. Kamble, N.M. Gupta, Catal. Lett. 88 (2003) 175.
[7] M. Fröba, R. Köhn, G. Bouffaud, Chem. Mater. 11 (1999) 2858.
[8] L.Z. Wang, J.L. Shi, W.H. Zhang, M.L. Ruan, J. Yu, D.S. Yan, Chem. Mater. 11 (1999) 3015.
[9] C.T. Kresge, M.E. Leonowicz, W.J. Roth, J.C. Vartuli, J.S. Beck, Nature 359 (1992) 710.
[10] C. Flego, A. Carati, C. Perego, Micropor. Mesopor. Mater. 44/45 (2001) 733.
[11] I.A. Fisher, A.T. Bell, J. Catal. 184 (1999) 357.
[12] T.R. Forester, R.F. Howe, J. Am. Chem. Soc. 109 (1987) 5076.
[13] G. Busca, A.S. Elmi, P. Forzatti, J. Phys. Chem. 91 (1987) 5263.
[14] G.J. Millar, C.H. Rochester, K.C. Waugh, J. Chem. Soc., Faraday Trans. 87 (1991) 2795.
[15] V. Lochař, J. Machek, J. Tichý, Appl. Catal. A: Gen. 228 (2002) 95.
[16] G.J. Millar, C.H. Rochester, K.C. Waugh, J. Chem. Soc., Faraday Trans. 87 (1991) 2785.